LETTERS

Daughter bubble cascades produced by folding of ruptured thin films

James C. Bird[1], Riëlle de Ruiter[1], Laurent Courbin[2] & Howard A. Stone[1,3]

Thin liquid films, such as soap bubbles, have been studied extensively for over a century because they are easily formed and mediate a wide range of transport processes in physics, chemistry and engineering[1–3]. When a bubble on a liquid–gas or solid–gas interface (referred to herein as an interfacial bubble) ruptures, the general expectation is that the bubble vanishes. More precisely, the ruptured thin film is expected to retract rapidly until it becomes part of the interface, an event that typically occurs within milliseconds[4–6]. The assumption that ruptured bubbles vanish is central to theories on foam evolution[7] and relevant to health[8] and climate[9] because bubble rupture is a source for aerosol droplets[10,11]. Here we show that for a large range of fluid parameters, interfacial bubbles can create numerous small bubbles when they rupture, rather than vanishing. We demonstrate, both experimentally and numerically, that the curved film of the ruptured bubble can fold and entrap air as it retracts. The resulting toroidal geometry of the trapped air is unstable, leading to the creation of a ring of smaller bubbles. The higher pressure associated with the higher curvature of the smaller bubbles increases the absorption of gas into the liquid, and increases the efficiency of rupture-induced aerosol dispersal.

A bubble-bursting cascade is illustrated experimentally in Fig. 1a–d. A hemispherical soap bubble, approximately four centimetres in diameter, is formed on a glass slide. Following rupture, a ring of smaller bubbles, each approximately a millimetre in diameter, appears around the base of the initial bubble (Fig. 1b). When one of these daughter bubbles ruptures, a ring of even smaller bubbles forms (Fig. 1d). Thus we observe a two-stage cascade, whereby one large bubble generates many smaller bubbles and so reduces the characteristic length scale over two orders of magnitude.

We believe that the physics responsible for this cascade generalizes beyond soap bubbles and provides an explanation for why, in the ocean, smaller bubbles are often observed after a larger sea bubble ruptures[11,12]. The importance of daughter bubbles for aerosol dispersion is highlighted in Fig. 1e–j. An air bubble is created on a pool of water collected from a local river (42.369° N, 71.122° W). Indigenous surfactants tend to be present in estuaries and oceans[13]; these natural surfactants stabilize the bubble, allowing a larger size and longer lifetime than would be observed with pure water. Eventually a hole nucleates on the bubble, causing the film to retract[4–6,13–19] and exposing the dimpled air–liquid interface to atmospheric pressure (Fig. 1f). The curved interface relaxes and propels a jet of liquid upward[10,20–23]. Around this jet is a ring of daughter bubbles (Fig. 1g). Within half a second, the daughter bubbles burst and propel droplets into the atmosphere (Fig. 1h–j). Thus, by forming numerous daughter bubbles, a single larger bubble significantly increases aerosol generation.

To examine how the daughter bubbles are formed, we film the collapse of the bubble with two synchronized high-speed cameras, one viewing from the side and the other from below (Fig. 2). The bubble is formed from a moderately viscous water–glycerol–sodium dodecyl sulphate solution to slow down the dynamics and stabilize the retracting rim. The high-speed images reveal that the daughter bubbles form in two distinct steps, each with a characteristic timescale. In the first step, the film collapses and folds such that air is trapped (Fig. 2a). The timescale over which the film retracts (about 3 ms) is consistent with inertially dominated film retraction[5,14]. In the second step, each torus of air becomes unstable and breaks up into a ring of daughter bubbles (Fig. 2b). This longer timescale (about 50 ms) is consistent with a capillary-driven phenomenon regulated by viscosity (see Supplementary Information).

From our observations in Fig. 2, we can understand the dynamics of the daughter bubble cascade. Prior to rupture, there is an equilibrium where capillary stresses on the curved surface are directed inward and are balanced by the outwardly directed bubble pressure. Once a hole nucleates in the thin film, the edge of the film retracts[5,14,15]. The compressed gas equilibrates instantaneously, that is, the pressure difference between the interior gas and the ambient vanishes, which results in a net inward force along the film due to capillary effects (see Supplementary Information). Meanwhile, the inertia of the liquid in the film leads to an outward trajectory of the moving rim. The combination of capillarity and inertia produces a folding of the film that entraps a torus of air. The torus itself, like other cylindrical fluid interfaces, is unstable to small perturbations and reduces surface energy by breaking into numerous small bubbles[3,24,25]. Provided that each of these smaller bubbles behaves similarly to the initial bubble, the process is iterative, creating a bubble-bursting cascade.

To test this mechanism for film folding, we next numerically simulated the film dynamics during retraction. Although retraction of planar films is well-studied, simulations capable of capturing the dynamics of curved films have not been studied systematically. Therefore, we developed a mathematical model of the inertial dynamics of a curved, retracting film (Supplementary Fig. 1). Our goal was to identify an elementary description that accurately reproduces the observed film dynamics. We assumed that the film thickness is initially uniform and that the resulting bubble collapse is axisymmetric. Following the formation of a hole in the film, the gas pressure inside the bubble equilibrates with the atmospheric pressure on a timescale of the order of 10 μs, which is set by the speed of sound. Surface tension drives the resulting collapse of the liquid film, whereas the inertia of the film regulates the motion. The simulations based on this model reproduce qualitative features of the experiments, but lack important details. These details are recovered when the simulations incorporate the internal pressure that results when the collapsing film squeezes the gas through the opening hole (Supplementary Fig. 2). The resulting shapes (Fig. 3a) are quantitatively similar to those observed experimentally (Fig. 2a). The collapse time and the initial film folding are accurately captured by the simulations.

[1]School of Engineering and Applied Sciences, Harvard University, Cambridge, Massachusetts 02138, USA. [2]Institut de Physique de Rennes, UMR CNRS 6251, Campus Beaulieu, Université Rennes 1, 35042 Rennes, France. [3]Department of Mechanical and Aerospace Engineering, Princeton University, Princeton, New Jersey 08544, USA.

©2010 Macmillan Publishers Limited. All rights reserved

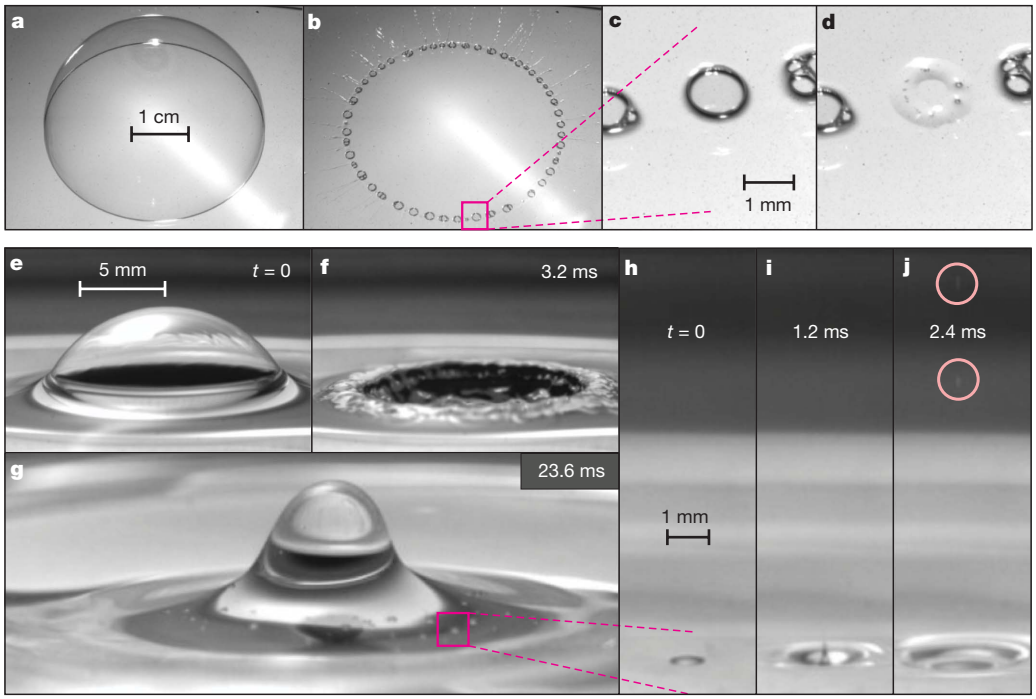

Figure 1 | The daughter bubble cascade, with jets, droplets and daughter bubbles resulting from bursting bubbles. **a**–**d**, When a single soap bubble ruptures on a rigid surface, a ring of many smaller bubbles can form. Similarly, when one of the daughter bubbles pops, even smaller bubbles are created, demonstrating a bubble-bursting cascade. **e**, The dynamics are more intricate when an air bubble ruptures on a deep pool of water. The Laplace pressure inside the bubble dimples the interface to create a cavity. **f**, Once the bubble ruptures, the film rapidly retracts (within a time $t = 3.2$ ms). **g**, As the cavity re-equilibrates, a jet of liquid is propelled upward. Many smaller daughter bubbles are visible around the jet. **h**–**j**, Within a fraction of a second, these secondary bubbles burst (**h**), a narrow jet forms (**i**), and tiny liquid droplets are dispersed into the atmosphere (**j**, inside pink circles). For more detail, see Supplementary Movies 1 and 2.

During the final moments of the collapse, it appears that the film can trap two separate pockets of air by folding on the lower surface and folding back on itself (Fig. 3b). The consequence of this folding is visible in Fig. 2b, where close inspection reveals the break-up of two rings of air that are concentric when viewed from above. If the rim of the film is unstable during retraction, the rim is observed to form threads and small drops, allowing the air to escape when the film folds onto itself (Fig. 3c). In this case, only one ring of daughter bubbles is produced, as experimentally demonstrated in Fig. 1b.

From our observations and simulations, we conclude that there are three conditions that control how much gas is entrapped in daughter bubbles produced by a bursting bubble: (1) the ability of the film to bend inward as it retracts, (2) the stability of the rim, and (3) the energy required to displace the initial gas inside the bubble. Our simulations demonstrate that the retraction of the film needs to be underdamped for the film to bend inward. Thus we expect daughter bubbles to form only when the inertial effects in the film are greater than the viscous effects, corresponding to a Reynolds number

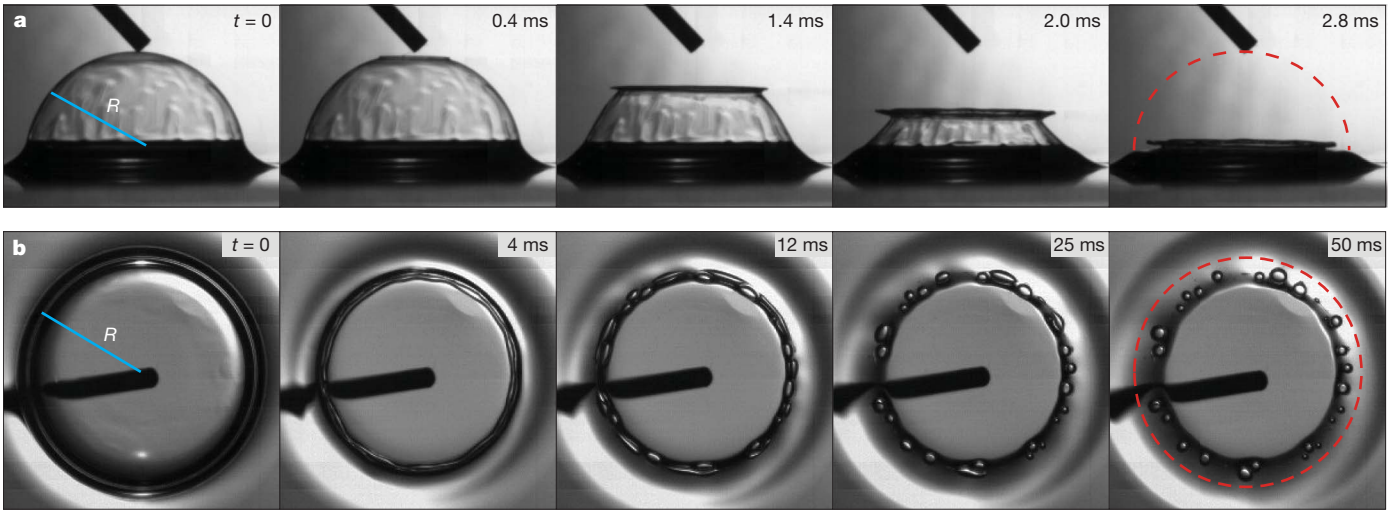

Figure 2 | Two-step mechanism to form daughter bubbles. **a**, High-speed images of a glycerol–water bubble filled with air popping on a solid surface viewed from the side. The bubble has an initial radius $R = 5.3$ mm, dynamic viscosity $\mu = 0.31$ Pa s, surface tension $\gamma = 55$ mN m^{-1}, and density $\rho = 10^3$ kg m^{-3}. **b**, The rupture is simultaneously filmed from below and reveals two concentric tori that break up into daughter bubbles. The red dotted lines in the final images denote the position of the bubble before rupture, and the time from rupture t is reported in milliseconds. For more detail, see Supplementary Movie 3.

©2010 Macmillan Publishers Limited. All rights reserved

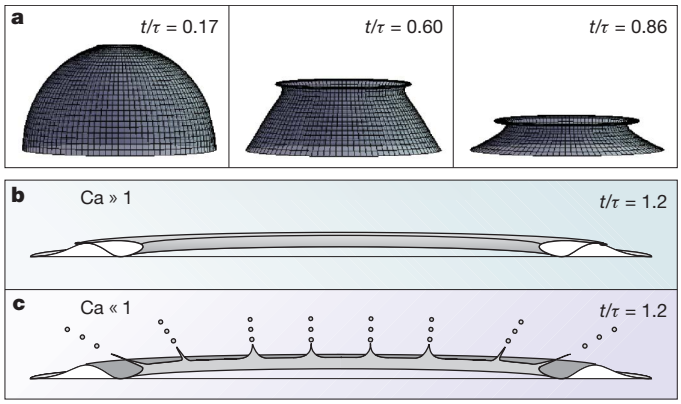

Figure 3 | Numerical simulations for understanding film folding and air entrapment. **a**, Our numerical simulation reproduces the inward folding behaviour of the collapsing film. The elapsed time t is dimensionalized by $\tau \equiv \sqrt{\rho R^2 h/\gamma}$. The selected times correspond to those in the three middle images in Fig. 2a with a film thickness of $h = 11\ \mu$m. **b**, A cross-sectional schematic of the proposed folding during the last stages of the collapse demonstrates how the film can create two concentric rings of air by intersecting with itself and the lower interface. This situation occurs when the capillary number is large $\mathrm{Ca} \equiv U\mu/\gamma \gg 1$. **c**, Another schematic illustrates how when the rim is unstable, the film traps only one torus of air. This rim instability appears to occur when $\mathrm{Ca} \ll 1$.

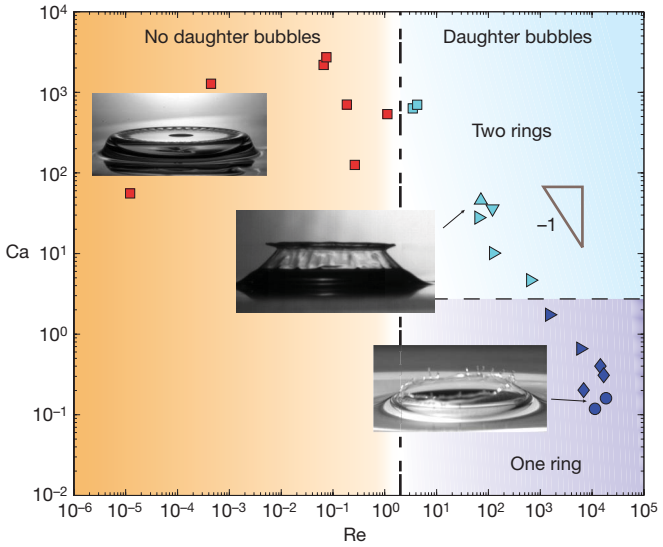

Figure 4 | Dynamical characterization of the formation of daughter bubbles. After a hemispherical bubble ruptures, there are either no daughter bubbles (red symbols), a single ring of daughter bubbles (blue symbols), or two concentric rings of daughter bubbles (cyan symbols). The transition between these regimes coincides with $\mathrm{Ca} \equiv U\mu/\gamma$ and $\mathrm{Re} \equiv \rho UR/\mu$ of approximately one, as predicted by our scaling arguments. The shapes of the data points correspond to various configurations: bubbles formed on deep pools of pure silicone oil (squares), on thin films of glycerol–water solutions stabilized by SDS surfactant (all triangles), and on deep pools of local river water stabilized by indigenous surfactant (circles and diamonds). The effects of different gases inside the bubbles were investigated using helium (right triangles and diamonds), nitrogen (up triangles), carbon dioxide (down triangles), and air (squares and circles).

$\mathrm{Re} = \rho RU/\mu \gg 1$, where ρ is the liquid density, R is the bubble radius, U is the characteristic retraction speed of the film (as measured experimentally), and μ is the liquid viscosity. The stability of the retracting rim depends on how the thickness of the film varies in the vicinity of the rim. Previously reported simulations for planar films find that the shape of the rim depends on both the Reynolds number and the capillary number, $\mathrm{Ca} = U\mu/\gamma$, where γ is the surface tension between the liquid and gas[17]. Specifically, the rim of a planar retracting film forms a distinct neck when both $\mathrm{Ca} \ll 1$ and $\mathrm{Re} \gg 1$, a condition that may cause the rim to break into tendrils and droplets. The instability of the rim appears to reduce the number of air torii from two to one, and the tendrils may even interfere with the remaining torus of air as it breaks up into daughter bubbles. Finally, our simulations suggest that the relative inertia between the gas and the film, $\rho_g R/(\rho h)$, where ρ_g is the gas density and h is the film thickness, influences the extent that the film folds inward and might therefore influence the size of the daughter bubbles (see Supplementary Information).

To test these predictions, we studied a set of bubbles with varying radius R and viscosity of the liquid μ over an extensive range, over nine and four orders of magnitude for Re and Ca respectively (Fig. 4). We also varied the density of the inner gas by blowing bubbles with helium, nitrogen and carbon dioxide. Three outcomes were observed: no daughter bubbles, one ring of daughter bubbles or two concentric rings of daughter bubbles (Fig. 4). Only when $\mathrm{Re} > 2$ are daughter bubbles observed, providing more evidence that inertial effects are critical to their formation. At sufficiently low Reynolds numbers, we observe an azimuthal instability in the collapsing film[6,18], yet this instability does not entrap air and no daughter bubbles are formed. Additionally, the transition between one and two rings occurs when $\mathrm{Ca} \approx 2$, supporting our hypothesis for instability of the rim. The density of the gas inside the bubble does not affect the number of rings obtained (Fig. 4), but we have observed that the specific gas does influence the average size of the daughter bubbles within the rings (see Supplementary Information).

The positions of the points in the bubble-bursting diagram (Fig. 4) provide additional insight into the film dynamics. At high Reynolds numbers, when viscosity is negligible, a uniform film retracts at a constant speed[5,14,15]: $U = \sqrt{2\gamma/(\rho h)}$. This expression provides an equation for the capillary number in terms of the Reynolds number, $\mathrm{Ca} = (2R/h)\mathrm{Re}^{-1}$. The data points follow this trend in the inertial regime with $2R/h \approx 1{,}000$ (Fig. 4). In contrast, when inertia is negligible ($Re \ll 1$), a uniform film retracts at an exponential rate with a characteristic speed[16] $U \propto R\gamma/(h\mu)$, which implies that at low Reynolds numbers, the capillary number follows $\mathrm{Ca} \propto R/h$. The dynamics are consistent with the data reported in the phase plot, and we attribute the slight scatter in Ca at low Re to variability in the relative film thickness. The transition between these two regimes ($Re \ll 1$ and $Re \gg 1$) coincides with the transition between no daughter bubbles and daughter bubbles (Fig. 4) and thus quantitatively rationalizes our observations.

Our results are relevant to the many fields that interfacial bubbles are already known to affect because we show that under certain conditions an initial bubble is a source for many smaller, more influential, bubbles. Aerosol droplets from bursting bubbles have been implicated in the transmission of diseases in swimming pools and hot tubs[8,26]. On a larger scale, sea spray, which transports dissolved gases, salt, thermal energy, and biological materials to the atmosphere and therefore influences climate, is largely attributed to aerosols produced by an estimated 10^{18} to 10^{20} bubbles that rupture every second across the oceans[9–11,27]. Before bursting, interfacial bubbles aerate the upper level of the ocean by increasing the adsorption of atmospheric gases into the water column[28]. In addition, interfacial bubbles can be problematic in industry, such as in glass manufacturing where air bubbles must be removed before the glass solidifies[29], and in biotechnology where the rapid liquid acceleration produced by a bursting bubble has been linked to cell mortality[30]. In these industrial processes where smaller bubbles, or the effects of small bubbles, are detrimental, understanding how these bubbles form is the first step in mitigation. We have quantified the limits of the folding behaviour and have shown that tuning the Reynolds and capillary numbers can suppress the formation of daughter bubbles. In situations where control of the interfacial properties is unrealistic, such as on the ocean surface, our study highlights the importance of larger bubbles in heat and mass exchange, as these bubbles can create many smaller bubbles each of which is capable of

©2010 Macmillan Publishers Limited. All rights reserved

dissolving gas into the water column and dispersing aerosols into the atmosphere.

Received 21 January; accepted 1 April 2010.

1. de Gennes, P. G., Brochard-Wyart, F. & Quéré, D. *Capillarity and Wetting Phenomena* (Springer, 2004).
2. Isenberg, C. *The Science of Soap films and Soap Bubbles* (Dover Publications, 1978).
3. Eggers, J. & Villermaux, E. Physics of liquid jets. *Rep. Prog. Phys.* **71,** 036601 (2008).
4. Dupré, A. Sixième mémoire sur la théorie mécanique de la chaleur. *Ann. Chim. Phys.* **11,** 194–220 (1867).
5. Taylor, G. I. The dynamics of thin sheets of fluid. III. Disintegration of fluid sheets. *Proc. R. Soc. Lond. A* **253,** 313 (1959).
6. Debrégeas, G., de Gennes, P. G. & Brochard-Wyart, F. The life and death of "bare" viscous bubbles. *Science* **279,** 1704–1707 (1998).
7. Weaire, D. & Hutzler, S. *The Physics of Foams* 144–150 (Clarendon Press, 1999).
8. Angenent, L. T., Kelley, S. T., St Amand, A., Pace, N. R. & Hernandez, M. T. Molecular identification of potential pathogens in water and air of a hospital therapy pool. *Proc. Natl Acad. Sci. USA* **102,** 4860–4865 (2005).
9. Wu, J. Evidence of sea spray produced by bursting bubbles. *Science* **212,** 324–326 (1981).
10. Woodcock, A. H., Kientzler, C. F., Arons, A. B. & Blanchard, D. C. Giant condensation nuclei from bursting bubbles. *Nature* **172,** 1144–1145 (1953).
11. MacIntyre, F. Flow patterns in breaking bubbles. *J. Geophys. Res.* **77,** 5211–5228 (1972).
12. Leifer, I., de Leeuw, G. & Cohen, L. H. Secondary bubble production from breaking waves: the bubble burst mechanism. *Geophys. Res. Lett.* **27,** 4077–4080 (2000).
13. Jarvis, N. L., Garrett, W. D., Scheiman, M. A. & Timmons, C. O. Surface chemical characterization of surface-active material in seawater. *Limnol. Oceanogr.* **12,** 88–96 (1967).
14. Culick, F. E. C. Comments on a ruptured soap film. *J. Appl. Phys.* **31,** 1128–1129 (1960).
15. Pandit, A. B. & Davidson, J. F. Hydrodynamics of the rupture of thin liquid-films. *J. Fluid Mech.* **212,** 11–24 (1990).
16. Debrégeas, G., Martin, P. & Brochard-Wyart, F. Viscous bursting of suspended films. *Phys. Rev. Lett.* **75,** 3886–3889 (1995).
17. Brenner, M. P. & Gueyffier, D. On the bursting of viscous films. *Phys. Fluids* **11,** 737–739 (1999).
18. da Silveira, R., Chaieb, S. & Mahadevan, L. Rippling instability of a collapsing bubble. *Science* **287,** 1468–1471 (2000).
19. Savva, N. & Bush, J. W. M. Viscous sheet retraction. *J. Fluid Mech.* **626,** 211–240 (2009).
20. Knelman, F., Dombrowski, N. & Newitt, D. M. Mechanism of the bursting bubble. *Nature* **172,** 261 (1954).
21. Boulton-Stone, J. M. & Blake, J. R. Gas-bubbles bursting at a free-surface. *J. Fluid Mech.* **254,** 437–466 (1993).
22. Zeff, B. W., Kleber, B., Fineberg, J. & Lathrop, D. P. Singularity dynamics in curvature collapse and jet eruption on a fluid surface. *Nature* **403,** 401–404 (2000).
23. Duchemin, L., Popinet, S., Josserand, C. & Zaleski, S. Jet formation in bubbles bursting at a free surface. *Phys. Fluids* **14,** 3000–3008 (2002).
24. Rayleigh, L. On the capillary phenomena of jets. *Proc. R. Soc. Lond.* **29,** 71 (1879).
25. Kendall, J. M. Experiments on annular liquid jet instability and on the formation of liquid shells. *Phys. Fluids* **29,** 2086–2094 (1986).
26. Blanchard, D. C. & Syzdek, L. Mechanism for the water-to-air transfer and concentration of bacteria. *Science* **170,** 626–628 (1970).
27. Baylor, E. R. Baylor, M. B., Blanchard, D. C., Syzdek, L. D. & Appel, C. Virus transfer from surf to wind. *Science* **198,** 575–580 (1977).
28. Farmer, D. M., McNeil, C. L. & Johnson, B. D. Evidence for importance of bubbles in increasing air-sea gas flux. *Nature* **361,** 620–623 (1993).
29. Beerkens, R. G. C. & van der Schaaf, J. Gas release and foam formation during melting and fining of glass. *J. Am. Ceram. Soc.* **89,** 24–35 (2006).
30. Handa, A., Emery, A. N. & Spier, R. E. On the evaluation of gas-liquid interfacial effects on hybridoma viability in bubble column bioreactors. *Dev. Biol. Stand.* **66,** 241–253 (1987).

Supplementary Information is linked to the online version of the paper at www.nature.com/nature.

Acknowledgements We thank P. Howell for discussions regarding our numerical simulations, and E. Villermaux and M. Brenner for feedback. We are grateful to the NSF via the Harvard MRSEC for support of this research.

Author Contributions J.C.B., L.C. and H.A.S. designed the research; J.C.B., R.d.R. and L.C. performed the research; J.C.B., R.d.R., L.C. and H.A.S. analysed the data; J.C.B. wrote the manuscript and all authors commented on it.

Author Information Reprints and permissions information is available at www.nature.com/reprints. The authors declare no competing financial interests. Readers are welcome to comment on the online version of this article at www.nature.com/nature. Correspondence and requests for materials should be addressed to J.C.B. (jbird@fas.harvard.edu) or H.A.S. (hastone@princeton.edu).

©2010 **Macmillan Publishers Limited. All rights reserved**